PROCEEDINGS A

rspa.royalsocietypublishing.org

Research

Cite this article: Mercier J-F, Maurel A. 2016 Improved multimodal method for the acoustic propagation in waveguides with a wall impedance and a uniform flow. *Proc. R. Soc. A* **472**: 20160094.
http://dx.doi.org/10.1098/rspa.2016.0094

Received: 8 February 2016
Accepted: 29 April 2016

Subject Areas:
applied mathematics, mathematical physics, acoustics

Keywords:
time harmonic, modal methods, acoustics in flows, multiple scattering

Author for correspondence:
Jean-François Mercier
e-mail: jean-francois.mercier@ensta-paristech.fr

Improved multimodal method for the acoustic propagation in waveguides with a wall impedance and a uniform flow

Jean-François Mercier[1] and Agnès Maurel[2]

[1] POEMS, ENSTA ParisTech, CNRS, Inria, Université Paris-Saclay, 828 bd des Maréchaux, 91762 Palaiseau Cedex, France
[2]Institut Langevin, CNRS, ESPCI ParisTech, 1 rue Jussieu, 75005 Paris, France

AM, 0000-0001-8432-9871

We present an efficient multimodal method to describe the acoustic propagation in the presence of a uniform flow in a waveguide with locally a wall impedance treatment. The method relies on a variational formulation of the problem, which allows to derive a multimodal formulation within a rigorous mathematical framework, notably to properly account for the boundary conditions on the walls (being locally the Myers condition and the Neumann condition otherwise). Also, the method uses an enriched basis with respect to the usual cosine basis, able to absorb the less converging part of the modal series and thus, to improve the convergence of the method. Using the cosine basis, the modal method has a low convergence, $1/N$, with N the order of truncation. Using the enriched basis, the improvement in the convergence is shown to depend on the Mach number, from $1/N^5$ to roughly $1/N^{1.5}$ for $M=0$ to M close to unity. The case of a continuously varying wall impedance is considered, and we discuss the limiting case of piecewise constant impedance, which defines pressure edge conditions at the impedance discontinuities.

1. Introduction

Guided waves have been subject to investigation for many years and they have a wide range of applications in engineering and physics [1,2] in the context of electromagnetic, [3,4] in acoustics, [5,6] in elasticity and [7–9] in the context of shallow oceans. For uniform and infinite waveguides, separation of variables

THE ROYAL SOCIETY PUBLISHING

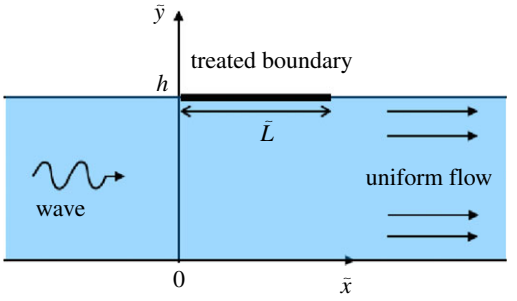

Figure 1. Waveguide with the upper wall characterized by a localized Myers boundary condition ($0 \leq \tilde{x} \leq \tilde{L}$), Neumann boundary condition otherwise.

is possible, and exact solutions of the guided wave propagation (called modes) exist. However, when longitudinal variations occur, the separability is in general lost. Modal methods are based on a series representation of the wavefield using the set of modes of the uniform waveguide. This has the advantage to recover simple solutions outside the non-uniform regions of the waveguide, where the modes are exact solutions. The numerical scheme has to describe the mode coupling inside the scattering regions and to account for the radiation condition and for the source condition. These multimodal methods have been shown to be computationally efficient in several contexts [10–12]. Efficient is meant here notably as: energy conservation and reciprocity are preserved and high convergence is obtained with respect to the number of modes used in the series representation. However, in several situations, the high convergences of modal methods are lost, and this is notably the case when the scattering region is due to a change in the boundary conditions. Degraded convergence has two origines. First, the mode coupling is encapsulated in a multimodal formulation whose expression is not unique, and this depends notably of how the boundary conditions are accounted for. In general, the different formulations are equivalent for non-truncated systems; however, it is not guaranteed that they lead to the same convergence rate for the truncated systems, as considered in practice. Next, because each mode does not satisfy the right condition at the walls, the solution, being a finite superposition of modes, behaves the same.

This paper addresses these two problems. First, the derivation of a multimodal formulation is proposed, which accounts for the boundary conditions unambiguously. In the present case, with the Myers boundary condition applying locally (figure 1), this is particularly involved, because tangential derivatives have to be accounted for (which makes direct projections on the transverse functions to fail). We show that a variational formulation solves this problem; besides, it makes continuous quantities appear, which are well suited for numerical implementations. It results that the best possible convergence is obtained when using the usual basis of cosine functions. This convergence can be further improved by enriching the basis of cosine functions with a so-called boundary mode. This new function has a non-zero derivative at the walls, and thus it allows to better approach the Myers boundary condition.

The paper is organized as follows. Because the presence of a flow induces specific complications not directly connected to the modal method, we first recall the main difficulties of the problem and the strategies proposed in the literature to solve them, §2. In §3, the derivation of the multimodal formulation, equation (3.20), is detailed. This is done by using the Prandtl–Glauert transformation, which allows to recover the usual Helmholtz equation while the boundary condition remains unaffected (thus, with no more and no less complexity). Although strictly speaking not necessary, this transformation allows for a simpler expression of the coupled mode equations. Next, a variational formulation of the problem allows to account properly for the boundary condition through two sets of modal components. It is an important aspect of our derivation that the boundary conditions are exactly taken into account, see also [13,14] where this approach has been used in other context of wave propagation. Section 3 ends with the

supplementary modal formulation (SupMF), built from the standard formulation (SMF) by means of an additional transverse function. Results on the convergences are presented in §4. Expectedly, the convergence of the classical modal formulation is low; for the scattering coefficients, it varies as $1/N$, and it is the best convergence that can be expected using the basis of cosine functions. The improved modal formulation restores a better convergence in $1/N^r$, and this improved convergence is found to depend on the Mach number M, namely from $1/N^5$ to $1/N^{1.5}$ for M increasing from 0 to a value close to unity. Our study is performed considering a continuous varying impedance, and we end inspecting the limiting case of a discontinuous impedance condition. In this case, the solution is found to tend towards a solution with a pressure being discontinuous at the impedance discontinuity, and with vanishing values at the interior boundaries of the impedance region. This may be useful to define additional edge condition, as it has been discussed in [15], when mode-matching approach is used.

Throughout the paper, a time dependence $\mathrm{e}^{-\mathrm{i}\omega t}$ is assumed (and this dependence is omitted).

2. General context of the acoustic propagation in treated waveguides in the presence of a flow

The propagation of waves in the presence of a flow is described by the linearized Euler equations, the linearization being performed for the acoustic quantities $(\rho, p, \mathbf{u})$, considered as small perturbations, around the base flow $(\rho_0, p_0, \mathbf{u}_0)$, with $(\rho_0, p_0, \mathbf{u}_0)$ being, respectively, the mass density, the pressure and the velocity. Next, assuming (i) that the base flow is uniform ($\mathbf{u}_0 = u_0\mathbf{e}_{\tilde{x}}$ in the $(\tilde{x}, \tilde{y})$ plane, and without loss of generality, we consider $u_0 \geq 0$) and (ii) that the acoustic velocity is irrotational, we get

$$-\Delta\phi + \tilde{D}^2\phi = 0, \tag{2.1}$$

for the velocity potential ϕ being defined by

$$\mathbf{u} = \boldsymbol{\nabla}\phi \quad \text{and} \quad p = -\tilde{D}\phi. \tag{2.2}$$

In equation (2.1), the operator $\tilde{D}$ is defined by

$$\tilde{D} \equiv M\frac{\partial}{\partial\tilde{x}} + \frac{1}{c}\frac{\partial}{\partial t}, \tag{2.3}$$

with the Mach number $M \equiv u_0/c$ and c the sound speed [16]. In the harmonic regime, $\tilde{D} = M\partial/\partial\tilde{x} - \mathrm{i}\tilde{k}$, with $\tilde{k} \equiv \omega/c$ the wavenumber. The hypothesis of irrotational flow is rather an approximation; strictly, the linearized Euler equations gives $\tilde{D}(\boldsymbol{\nabla} \times \mathbf{u}) = \mathbf{0}$, whose general solution is $\boldsymbol{\nabla} \times \mathbf{u} = \mathbf{A}(\tilde{y})\mathrm{e}^{\mathrm{i}\tilde{k}\tilde{x}/M}$. It is often argued that $\mathbf{A}$ vanishes if the incident vorticity (coming from $\tilde{x} \to -\infty$) vanishes. However, care has to be taken, because areas of discontinuities can generate free shear layers, which means that they can generate vorticity [17–20]. In this case, an additional complexity comes from the fact that the acoustic perturbation may interact with the base flow; this means that the acoustic energy is no longer conserved (see the appendix F in the ref. [16]).

If the flow is unbounded, an explicit solution of the problem can be found in the form of a combination of plane waves. In the simplest case of a solution being $\tilde{y}$-independent, the plane waves have simply a modified wavenumber $\tilde{k} \to \pm\tilde{k}/(1 \pm M)$ along $\tilde{x}$. Bounded configurations are of more practical interest: a flow along a wall (semi-infinite case in the $\tilde{y}$-direction) [21,22] or a flow in a waveguide (bounded in the $\tilde{y}$-direction) [18,23,24]. Again, if the walls bounding the space are uniformly rigid (associated with Neumann boundary conditions), the solution is simply a combination of plane waves with explicit solutions. Complications arise for more involved boundary conditions or when the boundary conditions on the walls vary, and this is the subject of this paper. This may correspond to inhomogeneities, as wall roughness, or wall treatments, and in some cases, such inhomogeneity along the walls can be encapsulated in an effective boundary condition. Obviously, the derivation of the equivalent boundary condition is

more or less involved, and it is a subject of research on its own. The problem has been regarded mainly in configurations with zero mean flow and are generally treated using homogenization techniques [25]. An exception is due to Myers [26], who derived an effective boundary condition in the presence of a flow (see also [16,22,27, §3.2.5]). This boundary condition accounts for the small vibration motion of an impenetrable compliant wall. Initially written in terms of the transverse displacement and the pressure, this condition ends with

$$\frac{\partial \phi}{\partial \tilde{y}} = \frac{1}{\mathrm{i}\tilde{k}} \tilde{D}(\tilde{Y}_0 \tilde{D}\phi), \tag{2.4}$$

on the wall, with $\tilde{Y}_0$ the surface admittance, proportional to the wall compliance. Note that in the absence of flow, the above relation gives a classical Robin condition. The Myers condition has been discussed in the context of efficient jump conditions at fluid–solid interfaces including prestress [28]. Also, it has been extensively used extending the notion of compliance to a series of closed tubes connected to the main waveguide (for which an effective compliance is used in the low-frequency regime) and this configuration is of practical interest for the applications to lined duct of turbo fan aircraft jet engine or to dissipative silencers with mean flow [29,30]. The resolution of the wave propagation in a waveguide whose walls have uniform impedance, equations (2.1)–(2.4), has been proposed in [31] using modal decomposition (and the modes are determined numerically in this case). When the walls have variable impedance, but piecewise constant, mode-matching approach has been used [15,32]. The modes are determined in each region with constant impedance, afterwards, the solution is matched at the interfaces between two regions. Complications arise in this case owing to the choice in the quantities that are assumed to be continuous. The case of continuously varying compliance has received less attention. We mention the recent work of Auregan & Pagneux [33], who considers a reduced one-dimensional problem involving the value of the potential at the wall and the average of the potential over the waveguide cross section. Once the dependence of the potential on the transverse direction has been chosen (with two degrees of freedom), the resolution along the axial direction is performed, leading to an approximate solution in the whole space. By construction, this approach does not address the form of the transverse modes and it avoids to question the problem of the modal decomposition.

Strictly speaking, a modal decomposition is always possible, being performed using the basis of transverse functions adapted to the boundary conditions on the walls or using any basis of transverse functions. The main advantage of using the adapted transverse functions is evident in the case of a uniform impedance condition; in this case, each mode is a solution of the problem on its own; for any source, the problem is a combination of modes that remain decoupled when propagate. In the case of piecewise constant impedance, the interest is less evident. On the one hand, the problem is simplified for the source being a finite combination of modes and for the radiation condition which applies on a decoupled system of modes. On the other hand, the matching of the solutions has to be done and this may become tricky, as previously said. Besides, this approach cannot be generalized to the case of a continuously varying impedance, and in fact, the notion of adapted transverse functions becomes fuzzy in that case. Note also that the completeness of the set of transverse functions is not demonstrated in the case of the wave equation in the presence of flow. This seems to plead in favour of the use of a known complete basis of transverse functions, as presented in the following sections.

3. Multimodal formulations

(a) Prandtl–Glauert transformation

We consider a waveguide of height h, with rigid walls except in a region of length $\tilde{L}$, acoustically treated and characterized by the admittance $\tilde{Y}_0(\tilde{x})$ (figure 1). The linearized Euler equations for

the velocity potential $\phi(\tilde{x},\tilde{y})$ lead to

$$(\Delta_{\tilde{x}\tilde{y}} - \tilde{D}^2)\phi = 0, \quad \text{in } \mathbb{R}\times]0,h[, \tag{3.1a}$$

$$\frac{\partial\phi}{\partial\tilde{y}} = 0, \quad \text{at } \tilde{y}=0, \tag{3.1b}$$

$$\frac{\partial\phi}{\partial\tilde{y}} = \frac{1}{\mathrm{i}\tilde{k}}\tilde{D}(\tilde{Y}_0\tilde{D}\phi), \quad \text{at } \tilde{y}=h,\ \tilde{x}\in[0,\tilde{L}] \tag{3.1c}$$

and

$$\frac{\partial\phi}{\partial\tilde{y}} = 0, \quad \text{at } \tilde{y}=h,\ \tilde{x}\notin[0,\tilde{L}], \tag{3.1d}$$

with

$$\left.\begin{aligned}\tilde{D} &= M\frac{\partial}{\partial\tilde{x}} - \mathrm{i}\tilde{k}\\ \text{and}\quad \Delta_{\tilde{x}\tilde{y}} &= \frac{\partial^2}{\partial\tilde{x}^2} + \frac{\partial^2}{\partial\tilde{y}^2}.\end{aligned}\right\} \tag{3.2}$$

The Lorentz or Prandtl–Glauert transformation is classically used to transform the wave equation in the presence of the flow to the Helmholtz equation [16]. This is done by using the new function $\varphi(x,y)$ such that

$$\phi(\tilde{x},\tilde{y}) = \varphi(x,y)\,\mathrm{e}^{\mathrm{i}\delta x},$$

with the new spatial variables $x=\tilde{x}/\beta$, $y=\tilde{y}$ and the parameters

$$\beta=\sqrt{1-M^2}, \quad \text{and} \quad \delta=-\tilde{k}M/\beta.$$

Starting from equation (3.1), such transformation leads to the problem

$$\left(\frac{\partial^2}{\partial x^2} + \frac{\partial^2}{\partial y^2} + k^2\right)\varphi = 0, \quad \text{in } \mathbb{R}\times]0,h[, \tag{3.3a}$$

$$\frac{\partial\varphi}{\partial y} = 0, \quad \text{at } y=0 \tag{3.3b}$$

and

$$\frac{\partial\varphi}{\partial y} = \left(M\frac{\partial}{\partial x} - \mathrm{i}k\right)\left[Y(x)\left(M\frac{\partial}{\partial x} - \mathrm{i}k\right)\varphi\right], \quad \text{at } y=h, \tag{3.3c}$$

where $k=\tilde{k}/\beta$ and $Y(x)$ is the extension of $Y_0(x)=\tilde{Y}_0(\tilde{x})$ to $\mathbb{R}$, specifically

$$\left.\begin{aligned}Y(x) &= \frac{\tilde{Y}_0(\beta x)}{\mathrm{i}k\beta^3} \quad \text{for } x\in\left[0, L=\frac{\tilde{L}}{\beta}\right]\\ \text{and}\quad Y(x) &= 0 \qquad\quad \text{for } x\notin[0,L],\end{aligned}\right\} \tag{3.4}$$

so that the boundary conditions (3.1*c*) and (3.1*d*) are encapsulated in the new equation (3.3*c*).

Remark 3.1. Note that problem (3.3) is not the initial problem (3.1) without flow. Indeed, $M=0$ in the Myers condition (3.1*c*) leads to the boundary condition $\partial\phi/\partial\tilde{y}=\mathrm{i}\tilde{k}\tilde{Y}_0\phi$ at $\tilde{y}=h$, with no tangential derivative, and thus different from the boundary condition in (3.3*c*). Therefore, the Prandtl–Glauert transformation has the advantage to lead to the Helmholtz equation in a fluid at rest but does not simplify the boundary condition. It keeps a boundary condition of the Myers type, with a double tangential derivative.

(b) The variational formulation

In the standard formulation, φ is expanded onto the set of the first N rigid transverse functions $u_n(y)$

$$\varphi(x,y)=\sum_{n=0}^{N-1}\varphi_n(x)u_n(y), \tag{3.5}$$

with

$$u_n(y)=\sqrt{\frac{2-\delta_{n0}}{h}}\cos\frac{n\pi y}{h},$$

which are orthogonal for the scalar product $(f,g)\equiv\int_0^h \mathrm{d}y f(y)\bar{g}(y)$.

The modal formulation can be obtained by projecting the wave equation onto the set of the transverse functions u_n, and accounting for the boundary conditions at some point. In the present case, this direct projection is not possible because of the second-order derivative in the Myers boundary condition. Alternatively, we will use the variational formulation of the problem (3.3). To anticipate, this approach has two advantages

— it reduces the order of derivation from 2 to 1, which notably makes the Myers condition more tractable,
— it gives the continuity conditions to apply along the x-axis for φ_n and its derivative

(3.6)

and this will be commented further in the following.

The variational formulation is obtained classically by introducing a test function ξ, which is chosen in the present case with separate variables $\xi(x,y)=\zeta(x)u_n(y)$, with $\zeta(x)$ a continuously derivable function compactly supported ($\zeta=0$ for $|x|>R$ with R any positive constant such that $R>L$). Such choice of the ζ function ensures that the integrals will be finite (the infinite integration domain $\mathbb{R}\times]0,h[$ is reduced to the bounded domain Ω_R corresponding to $|x|<R$) and to avoid any boundary term at infinity. Multiplicating equation (3.3*a*) by $\bar{\xi}$ and integrating over Ω, we get

$$\begin{aligned}\int_{\Omega_R}\left(\frac{\partial\varphi}{\partial x}\frac{\overline{\partial\xi}}{\partial x}+\frac{\partial\varphi}{\partial y}\frac{\overline{\partial\xi}}{\partial y}-k^2\varphi\bar{\xi}\right)\mathrm{d}x\,\mathrm{d}y&=\int_{\partial\Omega_R}(\boldsymbol{\nabla}\varphi\cdot\boldsymbol{n})\bar{\xi}\,\mathrm{d}x,\\&=\int_{|x|<R}\frac{\partial\varphi}{\partial y}(x,h)\bar{\xi}(x,h)\,\mathrm{d}x,\end{aligned}$$

where we have used the integration by parts of $\int_\Omega\Delta\varphi\bar{\xi}$ (when not specified, f denotes $f(x,y)$ for any function f). The boundary integral involves $\partial_y\varphi(x,h)$, and owing to the Myers boundary condition, equation (3.3*c*), we get after an integration by parts

$$\int_{\Omega_R}\left(\frac{\partial\varphi}{\partial x}\frac{\overline{\partial\xi}}{\partial x}+\frac{\partial\varphi}{\partial y}\frac{\overline{\partial\xi}}{\partial y}-k^2\varphi\bar{\xi}\right)\mathrm{d}x\,\mathrm{d}y+\int_{|x|<R}Y(x)\left(M\frac{\partial\varphi}{\partial x}-\mathrm{i}k\varphi\right)\left(M\frac{\overline{\partial\xi}}{\partial x}+\mathrm{i}k\bar{\xi}\right)\mathrm{d}x=B, \tag{3.7}$$

with the term

$$B=M\left[Y(x)\left(M\frac{\partial\varphi}{\partial x}-\mathrm{i}k\varphi\right)\bar{\xi}\right]_{x=0}^{x=L}, \tag{3.8}$$

appearing for non-continuous $Y(x)$ at $x=0,L$ (other discontinuities are disregarded) being a boundary term obtained after integration by parts on $x\in]0,L[$. Non-vanishing value of B may lead to significant complications. Physically speaking, it is associated with discontinuities in the fields (owing to Dirac functions). Mathematically, non-vanishing B may lead to an ill-posed problem; conversely, $B=0$ ensures that the problem is well posed [34]. In fact, $B=0$ for $Y(x)$ being continuous or not at 0 and L. Indeed, it has been shown in [34] that B cancels for $Y(0^+)\neq0$ and

$Y(L^-) \neq 0$, because the following relation is found

$$(M\partial\varphi/\partial x - \mathrm{i}k\varphi)(x = 0^+, h) = 0 = (M\partial\varphi/\partial x - \mathrm{i}k\varphi)(x = L^-, h).$$

This corresponds to the edge conditions on the pressure $p(0^+, h) = 0 = p(L^-, h)$ (see [15]), with

$$p(x, h) = -\left(M\frac{\partial\varphi}{\partial x} - \mathrm{i}k\varphi\right)(x, h), \tag{3.9}$$

from equation (2.2), and the edge conditions will be discussed further in §3c.

Finally, the variational formulation reads

$$\int_{\Omega_R}\left(\frac{\partial\varphi}{\partial x}\overline{\frac{\partial\xi}{\partial x}} + \frac{\partial\varphi}{\partial y}\overline{\frac{\partial\xi}{\partial y}} - k^2\varphi\bar{\xi}\right)\mathrm{d}x\,\mathrm{d}y + \int_{|x|<R} Y(x)\left(M\frac{\partial\varphi}{\partial x} - \mathrm{i}k\varphi\right)\left(M\overline{\frac{\partial\xi}{\partial x}} + \mathrm{i}k\bar{\xi}\right)\mathrm{d}x = 0. \tag{3.10}$$

This formulation is obtained for the velocity potential φ. In fact, one could think to derive a variational formulation for the pressure. This would lead to an additional difficulty. This is because the Myers boundary condition is of the form

$$\frac{\partial p}{\partial y}(x, h) = \left(M\frac{\partial}{\partial x} - \mathrm{i}k\right)^2 [Y(x)p(x, h)]. \tag{3.11}$$

The calculations are roughly the same, but the integration by parts in equation (3.7) involves a derivative of $Y(x)$. It follows that the limit towards a discontinuous Y becomes problematic [34]. Note that this is consistent with the edge conditions that are related to delta Dirac function (for discontinuous Y) in the boundary integral.

(c) The standard multimodal formulation

The aim is now to get a modal formulation starting from equation (3.10). Basically, the idea is to expand φ onto the basis u_m, equation (3.12), and with the choice of $\xi(x, y) = \zeta(x)u_n(y)$, a system of coupled equations on the φ_n will appear, which is called the modal formulation. But before doing so, let us come back to our previous remarks on the advantages of the variational formulation mentioned in (3.6).

In [34], it has been proven that equation (3.10) has a unique solution φ, with φ and its spatial derivatives in $L^2(\Omega_R) = \{f / \int_{\Omega_R} |f|^2 < \infty\}$. This guarantees that they can be expanded onto the set of u_n (specifically, the series converges); notably

$$\varphi = \sum_{m=0}^{\infty} \varphi_m(x)u_m(y). \tag{3.12}$$

On the contrary, the second spatial derivatives of φ are not in $L^2(\Omega_R)$, and thus, their expansions cannot be used, because the convergence of the series is not guaranteed. This is why it was important that the variational formulation reduces the order of derivation from 2 to 1. Also of practical importance is that, because $\partial_x\varphi$ and $\partial_y\varphi$ are in $L^2(\Omega_R)$, it is possible to derivate the series term by term, namely

$$\frac{\partial\varphi}{\partial x} = \sum_{m=0}^{\infty} \varphi_m'(x)u_m(y) \quad \text{and} \quad \frac{\partial\varphi}{\partial y} = \sum_{m=0}^{\infty} \varphi_m(x)u_m'(y), \tag{3.13}$$

with φ_n and $\varphi_n' \in L^2(]-R, R[)$. This implies that φ_n is continuous, but does not guaranty that $\varphi_n'(x)$ is continuous (and this is why an additional derivation with respect to x is not allowed *a priori*).

We can now come back to the derivation of the modal formulation. Using the expansions in equations (3.12)–(3.13) in equation (3.10), we get for $n = 0, \ldots, N-1$:

$$\int_{\mathbb{R}} \left[\varphi_n'\zeta' + \gamma_n^2\varphi_n\zeta - k^2\varphi_n\zeta\right] \mathrm{d}x + \mathtt{A}_{nm} \int_{\mathbb{R}} Y(x)[M^2\varphi_m'\zeta' + \mathrm{i}kM(\varphi_m'\zeta - \varphi_m\zeta') + k^2\varphi_m\zeta]\mathrm{d}x = 0, \quad (3.14)$$

where

$$\mathtt{A}_{nm} = u_n(h)u_m(h), \quad (3.15)$$

(see the explicit expression in appendix A) and where we have used $(u_m', u_n') = \gamma_n^2\delta_{mn}$ with $\gamma_n = n\pi/h$ (throughout the paper, the absence of sum symbols means that the Einstein summation convention has been used). Equation (3.14) can be re-written

$$\int_{\mathbb{R}} [\varphi_n' + Y\mathtt{A}_{nm}M(M\varphi_m' - \mathrm{i}k\varphi_m)]\zeta'\,\mathrm{d}x + \int_{\mathbb{R}} [-k_n^2\varphi_n + \mathrm{i}kY\mathtt{A}_{nm}(M\varphi_m' - \mathrm{i}k\varphi_m)]\zeta\,\mathrm{d}x = 0, \quad (3.16)$$

where $k_n^2 \equiv k^2 - \gamma_n^2$.

The last step towards a multimodal formulation requires to integrate by part the first integral in equation (3.16). This leads to an equation of the form $\int_{\mathbb{R}} F\zeta\,\mathrm{d}x = 0$ being satisfied for all ζ, from which $F = 0$ is deduced. This is obtained if no boundary terms appear in the integration by part, which means in the present case that the auxiliary function

$$\psi_n \equiv \varphi_n' + Y\mathtt{A}_{nm}M(M\varphi_m' - \mathrm{i}k\varphi_m) \quad (3.17)$$

is continuous.

In fact, this is the case for the following reasons. First, $\psi_n \in L^2(-R, R)$ because φ_m and φ_m' do (equation (3.13)). At this stage, this does not means that ψ_n is differentiable; however, using the derivatives in the distributional sense, by restricting to more regular test functions $\zeta \in C^\infty([-R, R])$, one gets from equation (3.16)

$$\psi_n' = -k_n^2\varphi_n + \mathrm{i}kY\mathtt{A}_{nm}(M\varphi_m' - \mathrm{i}k\varphi_m). \quad (3.18)$$

This is written in the distributional sense, which means that ψ_n' could contain delta Dirac functions, in particular if ψ_n was discontinuous. Here, it is not the case, again, because φ_m and φ_m' are in $L^2(-R, R)$ (in equation (3.18)), and thus $\psi_n' \in L^2(-R, R)$ also. Now, with both ψ_n and ψ_n' in $L^2(-R, R)$, we can conclude that ψ_n is continuous and differentiable in the (say, usual) sense of the functions.

It is remarkable that the variational formulation makes naturally appear the two functions φ_n and ψ_n and it proves that they are continuous. Without using a variational formulation approach, the auxiliary function ψ_n is not easy to guess.

Now, the modal formulation is nothing else that the equations (3.17)–(3.18), and they can be formulated in terms of the vectors of the modal components $\boldsymbol{\psi} \equiv (\psi_n)$ and $\boldsymbol{\varphi} \equiv (\varphi_n)$

$$\left.\begin{aligned} \boldsymbol{\psi} &= \mathtt{B}\frac{\mathrm{d}\boldsymbol{\varphi}}{\mathrm{d}x} - \mathrm{i}kYM\mathtt{A}\boldsymbol{\varphi} \\ \text{and} \qquad \frac{\mathrm{d}\boldsymbol{\psi}}{\mathrm{d}x} &= \mathtt{K}^2\boldsymbol{\varphi} + \mathrm{i}kY\mathtt{A}\left(M\frac{\mathrm{d}\boldsymbol{\varphi}}{\mathrm{d}x} - \mathrm{i}k\boldsymbol{\varphi}\right), \end{aligned}\right\} \quad (3.19)$$

with $\mathtt{B} = 1 + YM^2\mathtt{A}$ and $\mathtt{K}_{mn} = \mathrm{i}k_n\delta_{mn}$. Eliminating $\mathrm{d}\boldsymbol{\varphi}/\mathrm{d}x$ by using $\mathrm{d}\boldsymbol{\varphi}/\mathrm{d}x = \mathtt{B}^{-1}(\boldsymbol{\psi} + \mathrm{i}kYM\mathtt{A}\boldsymbol{\varphi})$, deduced from the first equation of (3.19), leads to the matrix form

$$\frac{\mathrm{d}}{\mathrm{d}x}\begin{pmatrix}\boldsymbol{\varphi}\\ \boldsymbol{\psi}\end{pmatrix} = \begin{pmatrix}\mathtt{C} & \mathtt{B}^{-1}\\ \mathtt{D} & \mathtt{C}^T\end{pmatrix}\begin{pmatrix}\boldsymbol{\varphi}\\ \boldsymbol{\psi}\end{pmatrix}, \quad (3.20)$$

where $\mathtt{C} = \mathrm{i}kYM\mathtt{A}\mathtt{B}^{-1}$, $\mathtt{D} = \mathtt{K}^2 + k^2Y\mathtt{A}\mathtt{B}^{-1}$ and $\mathtt{C}^T$ is the transposed matrix of $\mathtt{C}$ (not the adjoint matrix, because $Y \in \mathbb{C}$). This equation is solved taking into account the continuity of $\boldsymbol{\varphi}(x)$ and of $\boldsymbol{\psi}(x)$. Specifically, a Magnus scheme is implemented on the matrix $\mathtt{Z}$ defined as $\boldsymbol{\psi} \equiv \mathtt{Z}\boldsymbol{\varphi}$, and it is essential that $\mathtt{Z}$ is continuous, notably to properly account for the radiation condition and for the source term (the numerical method based on a Magnus scheme can be found in [12,14,35] and it is not discussed here). Here, this is ensured, because $\boldsymbol{\varphi}$ and $\boldsymbol{\psi}$ are continuous.

(d) The supplementary mode formulation

As previously said, the convergence of the modal method presented in the previous section is low, because the basis functions do not satisfy the Myers boundary condition. This is known to produce Gibbs oscillations, similar to the oscillations of a Fourier series approximating a discontinuous function. It has been shown in a series of papers that adding a transverse function with non-zero derivative on the boundary increases the convergence of the modal methods [36,37], and we have shown that this can be adapted to our modal formulation without any additional complexity in the numerical scheme [38–40].

The supplementary mode is called $\chi(y)$, and we choose

$$\chi(y) \equiv \sqrt{\frac{2}{h}} \cos \frac{\pi y}{2h}. \tag{3.21}$$

A key point is to build, from the function χ, a function $u_{-1}(y)$ being orthogonal to the $u_n(y)$, $n = 0, \ldots N-1$, of the usual basis (truncated in the numerics). It is easy to see that

$$u_{-1}(y) \equiv a_{-1} \left[\chi(y) - \sum_{n=0}^{N-1} \chi_n u_n(y) \right], \tag{3.22}$$

with $\chi_n \equiv (\chi, u_n)$ satisfies such requirement. Here, a_{-1} stands for proper normalization of u_{-1} ($\|u_{-1}\| = 1$). Finally, u_{-1} satisfies the relation $(u'_{-1}, u'_n) = \gamma_{-1}\delta_{-1,n}$, for $n = -1$ to $N-1$, with

$$a_{-1}^2 = \frac{1}{1 - \sum_{n=0}^{N-1} \chi_n^2} \quad \text{and} \quad \gamma_{-1}^2 = \frac{\|\chi'\|^2 - \sum_{n=0}^{N-1} \chi_n^2 \gamma_n^2}{1 - \sum_{n=0}^{N-1} \chi_n^2}.$$

Note that both a_{-1} and γ_{-1} depend on the truncation number N. Owing to the above properties, the new expansion

$$\varphi(x, y) = \sum_{n=-1}^{N-1} \varphi_n(x) u_n(y) \tag{3.23}$$

has exactly the same structure and properties as the standard modal expansion equation (3.5), with $-1 \le n, m \le (N-1)$. It follows that the projection of the wave equation (3.10) leads to the same matrix expression equation (3.20) as in the SMF. Besides, it has been shown in [38] that the supplementary mode behaves as an evanescent mode associated with a wavenumber $k_{-1}^2 = k^2 - \gamma_{-1}^2 < 0$. This is expected, because the supplementary mode has to vanish far from the scattering region (only the propagative rigid modes exist in the far field). It has also been checked that increasing the truncation N makes the supplementary mode more and more evanescent ($\gamma_{-1} \propto N$, see equation (2.12) of [38]).

4. Results

We consider the following continuous $\tilde{Y}_0(\tilde{x})$ function, namely

$$\tilde{Y}_0(\tilde{x}) = \begin{cases} Y_1 \sin^2\left(\dfrac{\pi \tilde{x}}{2\varepsilon}\right) & \text{if } 0 \le \tilde{x} \le \varepsilon, \\ Y_1 & \text{if } \varepsilon < \tilde{x} < \tilde{L} - \varepsilon, \\ Y_1 \sin^2\left(\dfrac{\pi\left(\tilde{L} - \tilde{x}\right)}{2\varepsilon}\right) & \text{if } \tilde{L} - \varepsilon \le \tilde{x} \le \tilde{L}, \end{cases} \tag{4.1}$$

with $Y_1 \in \mathbb{C}$. $\Re e(Y_1)$ being the energy absorption has to be positive. The parameter ε measures the transition length on which the admittance goes from zero to Y_1 (and $\tilde{Y}_0$ is symmetric with respect to $\tilde{x} = \tilde{L}/2$). The limit $\varepsilon \to 0$ leads to a piecewise constant surface admittance, and this case is discussed in §3c. As previously said, the coupled mode system (3.20) is solved using a Möbius–Magnus scheme, as described in [14,35]. A plane wave $\varphi^{(\mathrm{inc})}(x, y) = \mathrm{e}^{\mathrm{i}kx}$ (or $\mathrm{e}^{\mathrm{i}(\tilde{k}/1+M)\tilde{x}}$ (before the

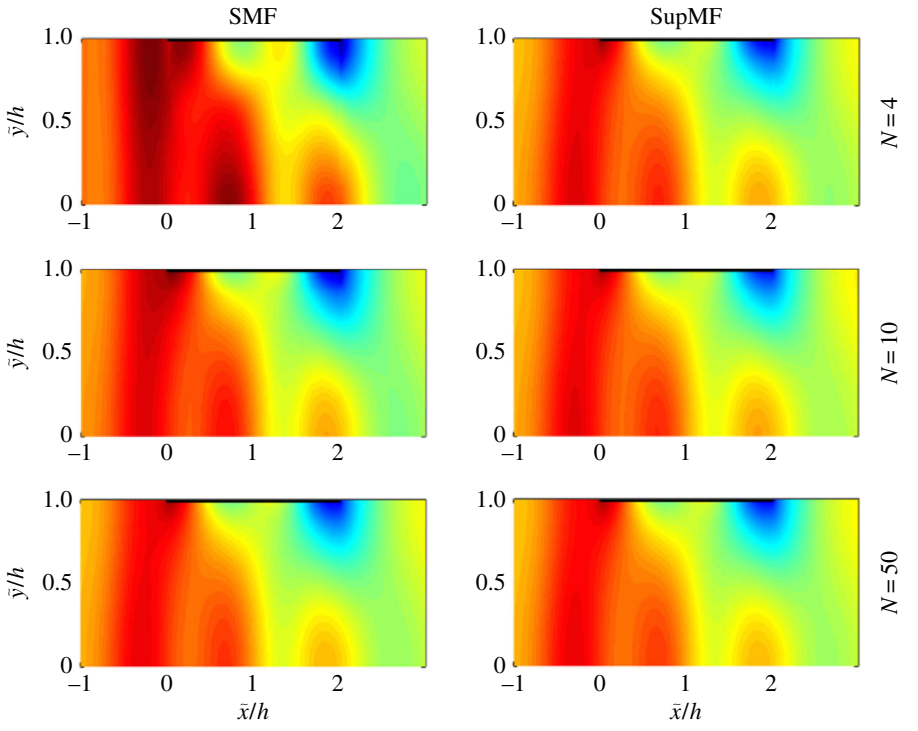

Figure 2. Wavefield (real part) in the waveguide, for $M = 0.7$, at frequency $\tilde{k}h = 2$, computed with the SMF (left panels) and SupMF (right panels) with $N = 4$, 10 and 50. The admittance is given by equations (4.1) with $Y_1 = 1 - 5\mathrm{i}$, $\varepsilon/h = 0.1$ and $\tilde{L}/h = 2$ (the part of the upper wall locally treated $0 < \tilde{x}/h < 2$ is materialized by a thick black line).

Prandtl–Glauert transformation has been applied) is sent from the left with the frequency $\tilde{k}h = 2$, and we choose $\tilde{L}/h = 2$, $\varepsilon/h = 0.1$. In this section, we compare the efficiencies of the SMF and of the SupMF.

(a) Results on the wavefield

In each formulation (SMF and SupMF), a field, that will be considered as converged, has been computed for a large N value ($N = 100$ in practice, and they have been validated by comparison with a finite-element method [34]). Next, the convergence of the two formulations is regarded for low truncations. Figure 2 shows the wavefields calculated with the SMF (left panels) and with the SupMF (right panels), for $N = 4$, 10 and 50 ($M = 0.7$, $Y_1 = 1 - 5\mathrm{i}$). Note that, in order to compare the two formulations with the same number of terms in the series, the summation has been done from $n = 0$ to $N - 1$ in the SMF and from $n = -1$ to $N - 2$ in the SupMF. The relative deviations between these fields and the converged fields are calculated by means of an integration over the whole domain (L^2-norm). In the SMF, they are 37% ($N = 4$), 15% ($N = 10$) and 4% ($N = 50$). The improvement in the SupMF is notable with 4% being already obtained for $N = 4$; increasing further N up to 50 produces a slight improvement, with 2% for $N = 10$ and close to 1% for $N = 50$ (however, no clear power law was found).

(b) Results on the scattering coefficients

In this section, the convergences of the two methods are further quantified by means of the convergences of the scattering coefficient R (reflection coefficient). At low frequency (here $\tilde{k}h = 2 < \pi$), only the plane wave mode is propagating and far enough from the scattering region, the

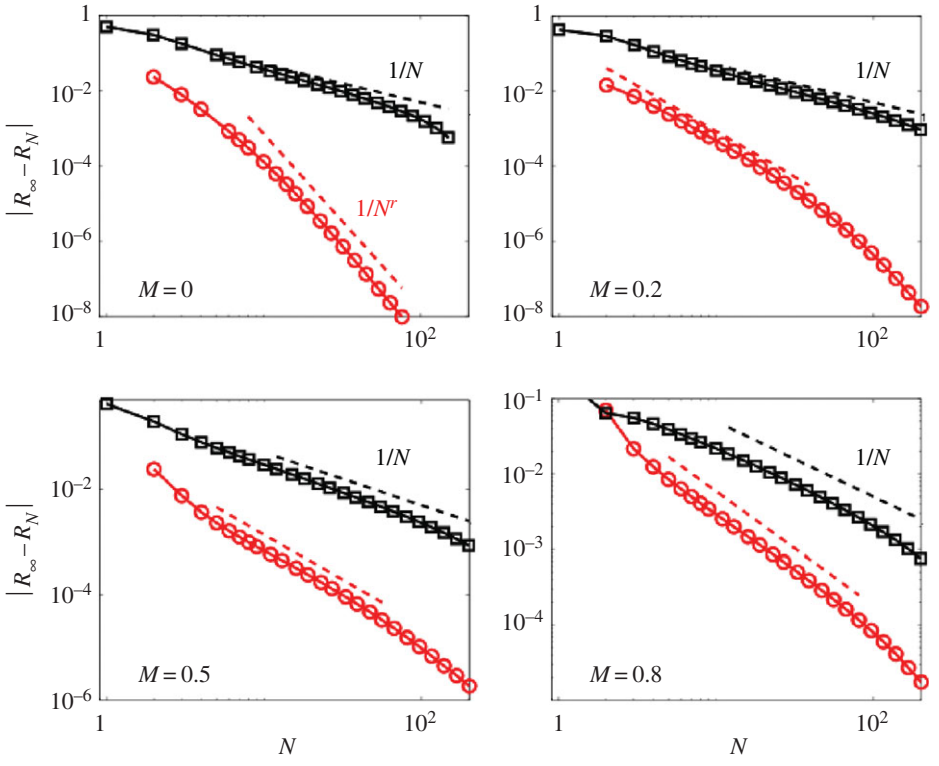

Figure 3. Error on the reflection coefficient, as a function of the truncation $N \leq 200$ for different Mach numbers M, $\tilde{kh} = 2$, $Y_1 = 5 - 5\mathrm{i}$, $\varepsilon/h = 0.1$ and $\tilde{L}/h = 2$. Squares, SMF; circles, SupMF. The reference R_∞ corresponds in practice to R_{500}. Dotted lines show power laws ($1/N$ in the SMF and $1/N^r$ in the SupMF, and $r(M)$ is obtained by a fit). (Online version in colour.)

field $p(x, y)$ reduces to

$$p(x \leq 0, y) = \mathrm{e}^{\mathrm{i}kx} + R\,\mathrm{e}^{-\mathrm{i}kx} \text{ and}$$
$$p(x \geq L, y) = T\,\mathrm{e}^{\mathrm{i}kx}.$$

The convergence of R is characterized by the behaviour of $|R_\infty - R_N|$ with N, as shown in figure 3 for increasing Mach values ($Y_1 = 5 - 5\mathrm{i}$ in the reported example). For $M = 0$, the rate of convergence is significantly improved: from $1/N$ in the SMF to $1/N^5$ in the SupMF, as already observed in [39], where the no flow case was considered. Next, increasing M, we still observe an improvement in the convergence but which is less and less significant.

For each M value, we have fitted the convergence rates r (for $|R_\infty - R_N| \propto 1/N^r$). In the SMF, it is $r = 1$ for any M, whereas in the SupMF, it decreases continuously, as reported in figure 4. It appears that the convergence rate r in the SupMF roughly follows $r = r_0 + r_1\,\mathrm{e}^{-\sigma M}$ with $r_0 \simeq 1.5$, $r_1 \simeq 3.1$ and $\sigma \simeq 5.6$ (plain line in figure 4). We have inspected the dependence of the coefficients (r_0, r_1, σ) on the value of Y_1, by varying the real and imaginary parts. We found that (r_0, r_1, σ) are rather constant. Nevertheless, for real parts of Y_1 becoming significantly smaller than the imaginary part (about $\frac{1}{10}$), we did not find a clear power law in the considered N-range. The real part of Y_1 is responsible of the dissipation, and it has already been observed in [39] (for the no flow case) that a vanishing dissipation produces significant surface modes near the treated region. These surface modes being associated with a small scale, it results that the convergence enters in a power law for an higher N-value (roughly speaking, once the small scale is resolved). The presence of the flow seems to make the presence of these small-scale structures more penalizing.

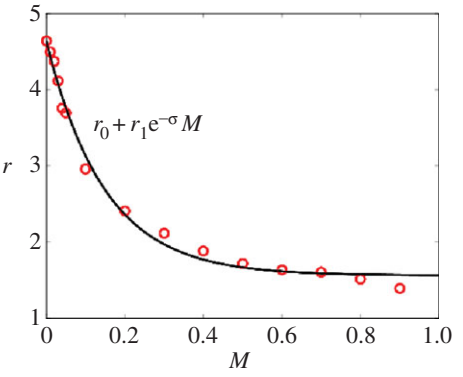

Figure 4. Variation of the convergence rate r with the Mach number in the SupMF formulation ($\tilde{k}h = 2$, $Y_1 = 5 - 5\mathrm{i}$, $\varepsilon/h = 0.1$ and $\tilde{L}/h = 2$). Circles: values of $r(M)$ calculated from the convergence curves (figure 3) with $|R_\infty - R_N| \sim 1/N^r$. Plain line: best fit of the data, with $r = r_0 + r_1\, e^{-\sigma M}$, leading to $r_0 = 1.5$, $r_1 = 3.1$ and $\sigma = 5.6$. (Online version in colour.)

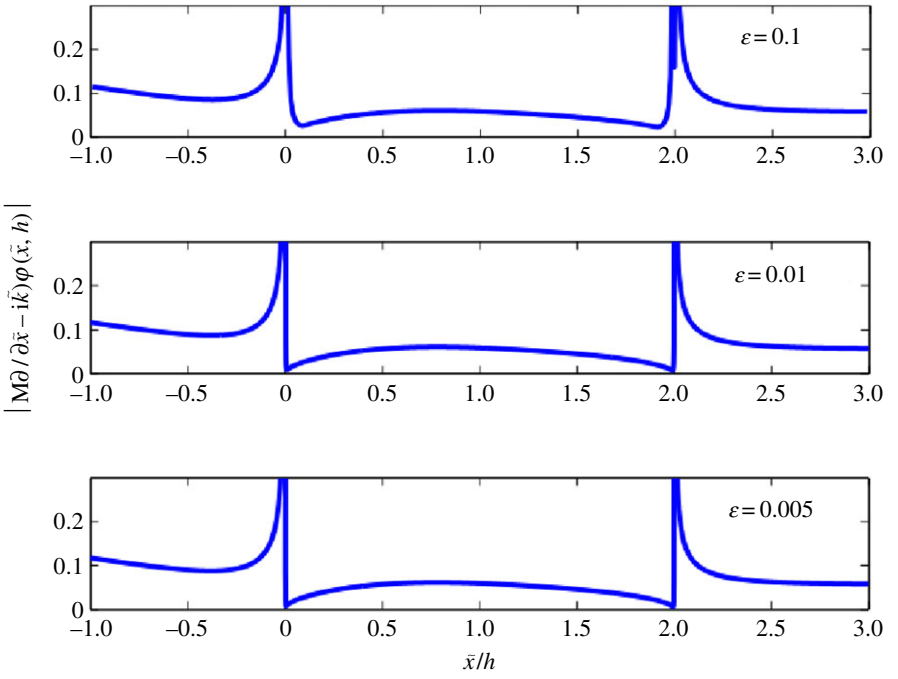

Figure 5. $|(M\partial/\partial\tilde{x} - \mathrm{i}\tilde{k})\varphi(\tilde{x}, h)|$ versus $\tilde{x}/h$ for three small ε values. $Y_1 = 1 - 5\mathrm{i}$, $M = 0.2$, $\tilde{L}/h = 2$ and $\tilde{k}h = 0.2$. Calculations have been done with $N = 20$. (Online version in colour.)

(c) The case of a discontinuous admittance

Because we have supposed that $Y(x)$ connects continuously to zero outside $[0, L]$, the case of a discontinuous Y function is disregarded (e.g. a piecewise constant Y function as considered in [41]). Nevertheless, it is of interest to consider the limit of vanishing transition region with $\varepsilon \to 0$ (incidentally, note that realistic discontinuous admittances coincide rather to this limit). Such approach is classical and it has been successfully used to establish appropriate matching conditions [15] or to derive the variational formulation of the potential problem, when both the base flow velocity and the acoustic velocity derive from scalar potentials [42]. In fact, it has already

been used in [34] for the present problem and it has been proved that edge conditions are found in the limit $\varepsilon \to 0$. Specifically, denoting φ_ε the solution of equation (3.10) for a transition length ε in equation (4.1), the limit $\varepsilon \to 0$ produces $\varphi_\varepsilon \to \varphi_0$, with φ_0 satisfying the edge conditions (or Kutta-like condition) $\tilde{D}\varphi_0(0^+,h) = 0 = \tilde{D}\varphi_0(\tilde{L}^-,h)$ (and $\tilde{D} = M\partial/\partial\tilde{x} - \mathrm{i}\tilde{k}$). With $p = -\tilde{D}\varphi$, equation (2.2), the edge conditions mean that the pressure vanishes at the end of the treated area.

We have reported in figure 5 the modulus of the pressure on the upper wall, by means of the convective derivative on the treated boundary $(M\partial/\partial\tilde{x} - \mathrm{i}\tilde{k})\varphi(\tilde{x},h)$ (the parameters are $M = 0.2$, $\tilde{k}h = 0.2$, $Y_1 = 1 - 5\mathrm{i}$ and $\tilde{L}/h = 2$). Decreasing the ε value produces a notable decrease of the pressure at the end of the treated region, as expected. Numerically, the pressure $p(0^-,h)$ and $p(\tilde{L}^+,h)$ do not tend to infinity when $\varepsilon \to 0$, and this was also theoretically expected [34], but clearly the pressure has strong discontinuities at $\tilde{x} = 0$ and $\tilde{x} = \tilde{L}$. Moreover, it is observed that both the velocity and the displacement potentials tend to continuous functions on the upper wall when $\varepsilon \to 0$ (figure not reported here): we recover the edge conditions of the mode-matching methods [15], which impose some regularity to the velocity or to the displacement, not to the pressure.

5. Conclusion

We have presented a modal method based on a variational formulation that perfectly accounts for the boundary conditions being locally of Myers type. This approach offers a rigorous mathematical framework, which permits to identify unambiguously the correct (which means notably continuous) quantities appearing in a first-order system, as used in modal formulations. This allows us to get the best convergence of the modal method, and we have further improved this convergence using an enriched modal basis. The improvement in the convergence rate is impressive for low Mach number, from $1/N$ to $1/N^5$ and it has been found that it is weaker for increasing M until being incidental for M close to unity. This limit $M \to 1$ is clearly singular, with $\beta \to 0$ producing a divergence of the admittance. In fact, the convected Helmholtz equation, equation (3.1*a*), is elliptic for $M < 1$ but becomes parabolic at $M = 1$. Thus, for M approaching 1, the variational formulation is less adapted (in fact, it fails for $M \geq 1$), and possibly also the modal formulation.

There are two natural extensions of this work. First, the extension to the asymmetric three-dimensional case that has been presented in details in the no flow case [39]; essentially, only the expression of the transverse functions is concerned from two- to three-dimension. Second, the extension to the case of a constant (instead of being vanishing) impedance outside the scattering region, say $Y = Y_2$ for $|x|$ large enough. In this case, the unique difficulty is to define the radiation condition (needed to initialize the Möbius–Magnus scheme).

In the case where $Y_2 = 0$, the radiation condition simply reads $\psi_n = ik_n\varphi_n$ whereas for $Y_2 \neq 0$, it has to be deduced from

$$\varphi_n'' + Y_2 \mathtt{A}_{nm} \left(M\frac{\mathrm{d}}{\mathrm{d}x} - \mathrm{i}k \right)^2 \varphi_m = K^2\varphi_n, \tag{5.1}$$

(from equations (3.19)), and this can be done by using the natural radiation condition corresponding to the diagonalized form of equation (3.20).

There are also two interesting extensions, but not straightforward. The first concerns the case of a shear flow $M(y)$, in particular because the convected Helmholtz equation is not valid anymore. Thus, the vectorial-linearized Euler equations have to be considered and the modal approach becomes tricky. In particular, one needs to use more sophisticated basis functions, for instance the Pridmore–Brown modes [43]. Also of interest is to consider alternative boundary conditions, which have been proposed to model accurately the sound absorption by liners under grazing flows, by accounting for the small but finite boundary layer on the liner [22,27] which is neglected in the Myers condition.

Ethics. In this study, we have not conducted any experiments on human beings or animals, nor used any collection of human or animal data.

Data accessibility. This work does not have any experimental data.

Authors' contributions. Both authors have participated in the reflection on the problem, they have set up the formalism and implemented the modal method.

Competing interests. We have no competing interests.

Funding. This work benefited from support of the French institutes INSIS and INSU of CNRS. A.M. is grateful for the support of LABEX WIFI (Laboratory of Excellence within the French Programme 'Investments for the Future') under references ANR-10-LABX-24 and ANR-10-IDEX-0001-02 PSL*.

Appendix A. Expressions of the matrix A

We give here the expression of

$$\mathtt{A}_{nm} \equiv u_n(h)u_m(h).$$

For the SMF, to get A (symmetric) it is sufficient to use

$$u_0(h) = \frac{1}{\sqrt{h}} \quad \text{and} \quad u_n(h) = \sqrt{2/h}(-1)^n.$$

For the SupMF, we need $u_{-1}(h) = -a_{-1}\sum_{n=0}^{N-1}\chi_n u_n(h)$ in addition (and $a_{-1} = 1/\sqrt{1-\sum_{n=0}^{N-1}\chi_n^2}$). It is thus sufficient to have χ_n

$$\chi_0 = \frac{2\sqrt{2}}{\pi} \quad \text{and} \quad \chi_n = \frac{4(-1)^{n+1}}{\pi(4n^2-1)}.$$

References

1. Collin RE. 1991 *Field theory of guided waves*, 2nd edn. Piscataway, NJ: IEEE Press.
2. Stevenson AF. 1951 General theory of electromagnetic horns. *J. Appl. Phys.* **22**, 1447–1460. (doi:10.1063/1.1699891)
3. Pagneux V, Amir N, Kergomard J. 1996 A study of wave propagation in varying cross-section waveguides by modal decomposition. I. Theory and validation. *J. Acoust. Soc. Am.* **100**, 2034–2048. (doi:10.1121/1.417913)
4. Adams SDM, Craster RV, Guenneau S. 2008 Bloch waves in periodic multi-layered waveguides. *Proc. R. Soc. A* **464**, 2669–2692. (doi:10.1098/rspa.2008.0065)
5. Pagneux V, Maurel A. 2005 Lamb wave propagation in elastic waveguides with variable thickness. *Proc. R. Soc. A* **462**, 1315–1339. (doi:10.1098/rspa.2005.1612)
6. Craster RV, Guenneau S, Adams SD. 2009 Mechanism for slow waves near cutoff frequencies in periodic waveguides. *Phys. Rev. B* **79**, 045129. (doi:10.1103/PhysRevB.79.045129)
7. Martin PA, Dalrymple A. 1994 On the propagation of water waves along a porous-walled channel. *Proc. R. Soc. A* **444**, 411–428. (doi:10.1098/rspa.1994.0029)
8. Linton CM, McIver P. 2007 Embedded trapped modes in water waves and acoustics. *Wave Motion* **45**, 16–29. (doi:10.1016/j.wavemoti.2007.04.009)
9. Cobelli PJ, Pagneux V, Maurel A, Petitjeans P. 2011 Experimental study on water-wave trapped mode. *J. Fluid Mech.* **666**, 445–476. (doi:10.1017/S0022112010004222)
10. Popov E, Nevière M. 2000 Grating theory: new equations in Fourier space leading to fast converging results fot TM polarization. *J. Opt. Soc. A* **17**, 1773–1784. (doi:10.1364/JOSAA.17.001773)
11. Maurel A, Mercier J-F, Pagneux V. 2014 Improved multimodal admittance method in varying cross section waveguide. *Proc. R. Soc. A* **470**, 20130448. (doi:10.1098/rspa.2013.0448)
12. Maurel A, Mercier J-F, Félix S. 2014 Wave propagation through penetrable scatterers in a waveguide and through a penetrable gratings. *J. Acoust. Soc. Am.* **135**, 165–174. (doi:10.1121/1.4836075)
13. Maurel A, Mercier J-F. 2012 Propagation of guided waves through weak penetrable scatterers. *J. Acoust. Soc. Am.* **131**, 1874–1889. (doi:10.1121/1.3682037)
14. Maurel A, Mercier JF, Félix S. 2015 Modal method for 2D wave propagation in heterogeneous anisotropic media. *J. Opt. Soc. Am.* **32**, 979–990. (doi:10.1364/JOSAA.32.000979)
15. Gabard G 2010 Mode-matching techniques for sound propagation in lined ducts with flow. In *Proc. 16th AIAA/CEAS Aeroacoustics Conf., Stockholm, Sweden, 7–9 June*. Reston, VA: AIAA.

16. Rienstra SW, Hirschberg A. 2004 *An introduction to acoustics*. Report IWDE 01-03. Eindhoven University of Technology. See http://exocomm.org/library/accoustics/boek.pdf.
17. Brambley EJ. 2009 Low-frequency acoustic reflection at a hard-soft lining transition in a cylindrical duct with uniform flow. *J. Eng. Math.* **65**, 345–354. (doi:10.1007/s10665-009-9291-1)
18. Rienstra SW. 2007 Acoustic scattering at a hard–soft lining transition in a flow duct. *J. Eng. Math.* **59**, 451–475. (doi:10.1007/s10665-007-9193-z)
19. Bonnet-Ben Dhia A-S, Dahi L, Lunéville E, Pagneux V. 2002 Acoustic diffraction by a plate in a uniform flow. *Math. Models Methods Appl. Sci.* **12**, 625–647. (doi:10.1142/S0218202502001829)
20. Job S, Lunéville E, Mercier J-F. 2005 Diffraction of an acoustic wave in a uniform flow: a numerical approach. *J. Comput. Acoust.* **13**, 689–709. (doi:10.1142/S0218396X05002840)
21. Brambley EJ, Gabard G. 2014 Reflection of an acoustic line source by an impedance surface with uniform flow. *J. Sound Vib.* **333**, 5548–5565. (doi:10.1016/j.jsv.2014.05.026)
22. Rienstra S, Darau M. 2011 Boundary-layer thickness effects of the hydrodynamic instability along an impedance wall. *J. Fluid Mech.* **671**, 559–573. (doi:10.1017/S0022112010006051)
23. Gabard G, Astley RJ. 2008 A computational mode-matching approach for sound propagation in three-dimensional ducts with flow. *J. Acoust. Soc. Am.* **315**, 1103–1124. (doi:10.1016/j.jsv.2008.02.015)
24. Gabard G. 2013 A comparison of impedance boundary conditions for flow acoustics. *J. Sound Vib.* **332**, 714–724. (doi:10.1016/j.jsv.2012.10.014)
25. Bonnet-Bendhia AS, Drissi D, Gmati N. 2004 Simulation of muffler's transmission losses by a homogenized finite element method. *J. Comput. Acoust.* **12**, 447–474. (doi:10.1142/S0218396X04002304)
26. Myers M. 1980 On the acoustic boundary condition in the presence of flow. *J. Acoust. Soc. Am.* **71**, 429–434. (doi:10.1016/0022-460x(80)90424-1)
27. Brambley E. 2011 Well-posed boundary condition for acoustic liners in straight ducts with flow. *AIAA J.* **49**, 1272–1282. (doi:10.2514/1.J050723)
28. Treyssede F, Tahar MB. 2009 Jump conditions for unsteady small perturbations at fluid–solid interfaces in the presence of initial flow and prestress. *Wave Motion* **46**, 155–167. (doi:10.1016/j.wavemoti.2008.10.003)
29. Kirby R, Denia FD. 2007 Analytic mode matching for a circular dissipative silencer containing mean flow and a perforated pipe. *J. Acoust. Soc. Am.* **122**, 71–82. (doi:10.1121/1.2793614)
30. Kirby R. 2009 A comparison between analytic and numerical methods for modeling automotive dissipative silencers with mean flow. *J. Acoust. Soc. Am.* **325**, 565–582. (doi:10.1016/j.jsv.2009.03.032)
31. Bonnet-Ben Dhia A-S, Mercier J-F, Redon E, PoernomoSari S. 2011 Non-reflecting boundary conditions for acoustic propagation in ducts with acoustic treatment and mean flow. *Int. J. Numer. Methods Eng.* **86**, 1360–1378. (doi:10.1002/nme.3108)
32. Rienstra S, Peake N 2005 Modal scattering at an impedance transition in a lined flow duct. In *11th AIAA/CEAS Aeroacoustics Conf., Monterey, CA, 23–25 May*. Reston, VA: AIAA.
33. Auregan Y, Pagneux V 2015 Slow sound in lined flow ducts. (http://arxiv.org/abs/1502.07883)
34. Lunéville E, Mercier J-F. 2014 Mathematical modeling of time-harmonic aeroacoustics with a generalized impedance boundary condition. *Math. Model. Numer. Anal.* **48**, 1529–1555. (doi:10.1051/m2an/2014008)
35. Félix S, Maurel A, Mercier J-F. 2014 Local transformation leading to an efficient Fourier modal method for perfectly conducting gratings. *J. Opt. Soc. Am. A* **31**, 2249–2255. (doi:10.1364/JOSAA.31.002249)
36. Athanassoulis GA, Belibassakis KA. 1999 A consistent coupled-mode theory for the propagation of small-amplitude water waves over variable bathymetry regions. *J. Fluid Mech.* **389**, 275–301. (doi:10.1017/S0022112099004978)
37. Athanassoulis GA, Belibassakis KA 2013 Rapidly-convergent local-mode representations for wave propagation and scattering in curved-boundary waveguides. *In Proc. 6th Int. Conf. on Mathematical and Numerical Aspects of Wave Propagation* (*waves* 2003), *Jyväskylä, Finland, 30 June–4 July 2003*, pp. 451–456. Berlin Heidelberg, Germany: Springer-Verlag.
38. Mercier J-F, Maurel A. 2013 Acoustic propagation in non uniform waveguides: revisiting Webster equation using evanescent boundary modes. *Proc. R. Soc. A* **469**, 20130186. (doi:10.1098/rspa.2013.0186)

39. Félix S, Maurel A, Mercier J-F. 2015 Improved multimodal methods for the acoustic propagation in waveguides with finite wall impedance. *Wave Motion* **54**, 1–10. (doi:10.1016/j.wavemoti.2014.11.007)
40. Maurel A, Mercier J-F, Félix S. 2014 Propagation in waveguides with varying cross-section and curvature: a new light on the role of supplementary modes in multimodal methods. *Proc. R. Soc. A* **470**, 20130743. (doi:10.1098/rspa.2013.0743)
41. Bi W, Pagneux V, Lafarge D, Aurégan Y. 2007 An improved multimodal method for sound propagation in non uniforms lined ducts. *J. Acoust. Soc. Am.* **122**, 280–290. (doi:10.1121/1.2736785)
42. Eversman W. 2001 The boundary condition at an impedance wall in a non-uniform duct with potential mean flow. *J. Acoust. Soc. Am.* **246**, 63–69. (doi:10.1006/jsvi.2000.3607)
43. Pridmore Brown DC. 1958 Sound propagation in a fluid flowing through an attenuating duct. *J. Acoust. Soc. Am.* **30**, 670–670. (doi:10.1121/1.1929943)